Local modal filters for automated data-based damage localization using ambient vibrations

G. Tondreau*, A. Deraemaeker

ULB, Service BATir, 50 av Franklin Roosevelt, CP 194/2, B-1050 Brussels, Belgium

ARTICLE INFO

ABSTRACT

The motivation of the paper is to develop a fully automated data-based technique for damage localization using in-service ambient vibrations. The idea is an extension of the modal filtering technique previously developed for damage detection. A very large network of dynamic strain sensors is deployed on the structure to be monitored and split into several independent local sensor networks. Simple and fast signal processing techniques are coupled to statistical control charts for efficient and fully automated damage localization. The efficiency of the method is demonstrated using time-domain simulated data on a simply supported beam and a three-dimensional bridge structure. The method is able to detect and locate very small damages (2% stiffness reduction in an area corresponding to 1/100th of the length of the structure) even in the presence of noise on the measurements and variability of the baseline structure.

1. Introduction

In many domains of engineering such as civil, mechanical and aerospace, assessing the integrity of the structures in (near) real time is a very important topic for which many methods have been developed in the last decades. Today, structural health monitoring (SHM) is gaining increasing attention: in the case of bridges for example, the maximum loads tend to increase (increase of the vehicle weights) while most of the structures are coming to the end of their theoretical lifetime (due to corrosion, fatigue loading, etc.). In [8], a broad overview of the problems which occurred on the East River Bridges in New York City due to their aging is given. Those phenomena as well as exceptional events such as collisions or earthquakes will possibly be responsible for a damage growth in the structures. Optimal maintenance calls for an early detection of small damages in structures, as it is well known that small and frequent repairs are much less costly than major repairs or total rebuilding after collapse. Current monitoring practice consists in scheduled maintenances including visual inspections, ultrasounds, eddy current, magnetic field or radiography techniques to name but a few [14]. All these experimental methods require however that the vicinity of the flaw is known, and that the proximity to be inspected is accessible. Moreover, these local inspections are tedious, expensive (the biennal inspection of the Brooklyn Bridge in New York lasts for more than three months and costs about one million US dollars [8]), subjective and not automated. In [8,21], the authors describe some of the difficulties encountered with the scheduled maintenance of long-span bridges. A major problem is that traditional monitoring is non-continuous which means that if a critical damage occurs between two

* Corresponding author. Tel.: +32 477468520.
 E-mail addresses: gilles.tondreau@ulb.ac.be (G. Tondreau), aderaema@ulb.ac.be (A. Deraemaeker).
 URL: http://batir.ulb.ac.be/ (G. Tondreau).

inspections, it might lead to catastrophic structural failure. One of the most relevant examples is the I-35W Mississippi River Bridge case [28]: this bridge collapsed in August 2007 killing 13 people and injuring 145, despite annual inspection.

A general trend for new structures and bridges is a lighter and more slender design, which tends to increase the levels of vibrations under ambient excitation. While these levels of vibrations need to be controlled as they could be detrimental to the lifetime of the structure, they can also be used for the continuous monitoring of the structure without disruption or decrease of functionality. The basic idea is that the occurrence of damage alters the structural parameters (i.e. corrosion of steel reinforcement decreases the stiffness in concrete structures, cracks create new surfaces which increase the damping [1] and alter the stiffness, etc.) which in turn affect the vibration characteristics. Based on this basic concept, many vibration based SHM techniques have been developed in the last decades using mainly eigenfrequencies, damping ratios or mode shapes [7]. The reason of this popularity is the ease of measuring modal parameters or frequency responses on real structures thanks to recent advances in sensing systems (increase of cost-effective computing memory and speed [16,33,35]).

The general SHM methodology can be decomposed in four levels [30], targeting the detection (level 1), the location (level 2) and the quantification (level 3) of the damage, as well as the prediction of the remaining service life of the damaged structure (level 4). As the level increases, the knowledge about the damage increases and, usually, the complexity of the method increases as well. The simplest methods are data-based methods. These methods present the important advantage of avoiding the need to construct a detailed numerical model of the structure to be monitored. A distinction must be made between unsupervised methods in which only data from the undamaged structure is available, and supervised methods for which data in different damage conditions is available as well. Generally, unsupervised methods are able to tackle the first level of SHM only, while supervised techniques can reach up to level 3. More complicated methods use model updating techniques and can reach up to level 4 [23,27,12]. Despite the huge scientific literature on the subject [34,7], SHM technologies for civil engineering structures have not yet been successful in real industrial applications, due to major difficulties. The first one is that the damage is typically a local phenomenon, which means that only important damage levels will be detected if one looks at global dynamic properties such as the eigenfrequencies [31]. The second one is that the structures are subjected to ambient excitation such as traffic or wind (which is changing and cannot be measured) as well as environmental changes (temperature, humidity). The vibration levels are rather low and instrumentation has to be very sensitive in order to measure them with a good accuracy. The third one is the problem of automation and robustness of the SHM system against sensor failure and variability (environment, loading, etc.) [15]. In addition, non-technical issues such as economic benefits that can be expected from SHM systems have to be further investigated in order to convince structure owners of the interest of such approaches.

In this paper, the authors propose an automated output-only method for the localization of small damages which fits particularly well to civil engineering applications. The method is divided into four steps, following the statistical pattern recognition paradigm proposed in [10]. Because the technique exploits only sensor responses, it falls in the category of data-based or non-model-based methods, therefore avoiding the need to build an accurate numerical model of the structure to be monitored, and relies on output-only in-service vibration data. This is motivated by the fact that, on one hand, many studies have shown that output-only measurements are representative of the dynamic behavior of the structure and can be used for modal identification [24,25], and that, on the other hand, the complexity of bridges and buildings is such that when constructing numerical models, the modeling errors are usually of an order of magnitude larger than the effect of damage on the dynamic properties (except if the damage is really severe). The method is based on a very simple and automated feature extraction process based on the so-called modal filters [4]. These features have been shown to be relatively robust to environmental changes [5] which can cause significant changes in modal properties [11]. Control charts [18,29] are used to detect automatically a change from the normal healthy condition, based on the extracted features. The automation of the process is a key point for a successful implementation of continuous monitoring systems.

This paper is organized as follows: Section 2 describes the method proposed for automated damage localization using output-only measurements. The theory of modal filters is briefly recalled, and the extension of the method proposed earlier for damage detection in [4] to damage localization is presented. Feature extraction and novelty detection using control charts are also detailed. Section 3 presents two numerical applications of the method: the first example is a simply supported beam. A comparison of damage localization possibilities using accelerations or dynamic strain measurements is presented, showing much better performances with dynamic strains. A second example of a more realistic bridge-like structure in which fiber optics FBGs (Fiber Bragg Grating sensors) are embedded is presented. Both examples exploit numerically simulated time-domain data (polluted with noise) obtained from finite element models, and show the very good potential performances of the proposed method.
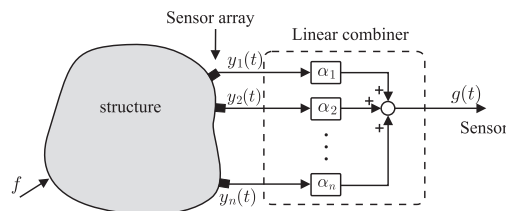

Fig. 1. Principle of spatial filtering on a network of n sensors.

2. Damage localization using modal filters

Initially developed for damage detection in [41,4], the modal filters concept as well as feature extraction are recalled in the present section. The extension of modal filters to an automated damage localization is then explained.

2.1. Data reduction using spatial filters and modal filters

Consider a structure equipped with a network of n sensors y_k and excited with a force f as depicted in Fig. 1. The modal expansion of the frequency response function (FRF) of the response on sensor k (considering N mode shapes) is given by

$$Y_k(\omega) = \sum_{i=1}^{N} \frac{c_{ki} b_i}{(\omega_i^2 - \omega^2 + 2j\xi_i\omega_i\omega)} \tag{1}$$

where c_{ki} is the modal output gain of sensor k, b_i is the modal input gain, ω_i is the ith angular natural frequency and ξ_i the modal damping of mode i. When the number of sensors is very large, it is interesting to perform data reduction in order to decrease the power consumption and the bandwidth needed to transmit the data, and to facilitate the data storage and post-processing. For SHM applications, an optimal reduction is one that significantly reduces the amount of data while keeping most of the information about the damage. A simple data reduction technique is spatial filtering [4]. The basic principle is illustrated in Fig. 1.

It consists in condensing the data from a network of n sensors through a linear combination to form a single output response:

$$g(t) = \sum_{k=1}^{n} \alpha_k y_k(t). \tag{2}$$

The corresponding FRF is

$$G(\omega) = \sum_{k=1}^{n} \alpha_k Y_k(\omega) = \sum_{i=1}^{N} \frac{\{\sum_{k=1}^{n} \alpha_k c_{ki}\} b_i}{(\omega_i^2 - \omega^2 + 2j\xi_i\omega_i\omega)} \tag{3}$$

The idea behind modal filtering is to choose the coefficients of the linear combiner α_k in such a way that they are orthogonal to all the modes of the structure in a frequency band of interest, except mode l [39,40]:

$$\sum_{k=1}^{n} \alpha_k c_{ki} = \delta_{li} \tag{4}$$

or in a matrix form:

$$[C]^T \{\alpha\} = e_l, \tag{5}$$

where $\{\alpha\} = \{\alpha_1 \cdots \alpha_n\}^T$ and $e_l = \{0\ 0 \cdots 1 \cdots 0\ 0\}^T$ (all components set to 0 except the lth component). The modal filter can be tuned to any of the N mode shapes of the structure. Once the modal filter coefficients α_k are defined, the linear combination is performed in time domain. In the frequency domain, the FRF of the modal filter tuned on mode l is given by

$$G(\omega) = \frac{b_l}{(\omega_l^2 - \omega^2 + 2j\xi_l\omega_l\omega)} \tag{6}$$

Note that because the modal filtering principle is based on Eq. (4), it is still applicable if the output sensors are velocities or accelerations.

2.2. Effect of damage and environment on modal filters

Suppose now that a structural change occurs. This will change the filtered frequency response $G(\omega)$ as follows:

$$G^*(\omega) = \sum_{k=1}^{n} \alpha_k Y_k^*(\omega) = \sum_{i=1}^{N} \frac{\{\sum_{k=1}^{n} \alpha_k c_{ki}^*\} b_i^*}{(\omega_i^{*2} - \omega^2 + 2j\xi_i^*\omega_i^*\omega)}, \tag{7}$$

where * refers to the properties of the modified structure. The structural change will affect the following quantities:

- b_i^*: change of the modal input gain;
- ω_i^* and ξ_i^*: changes of the eigenfrequencies and the modal damping;
- c_{ki}^*: change of the mode shapes. Depending on the nature of the mode shape change, the effect on the modal filter differs. If the mode shape change is local, Eq. (4) is not satisfied anymore:

$$\sum_{k=1}^{n} \alpha_k c_{ki}^* \neq \delta_{li} \tag{8}$$

In that case, the modal filter does not perfectly work and the filtered peaks might reappear around eigenfrequencies ω_i with $i \neq l$ (see Fig. 2 (a)). On the other hand, for global changes of the mode shapes, the appearance of peaks is much less
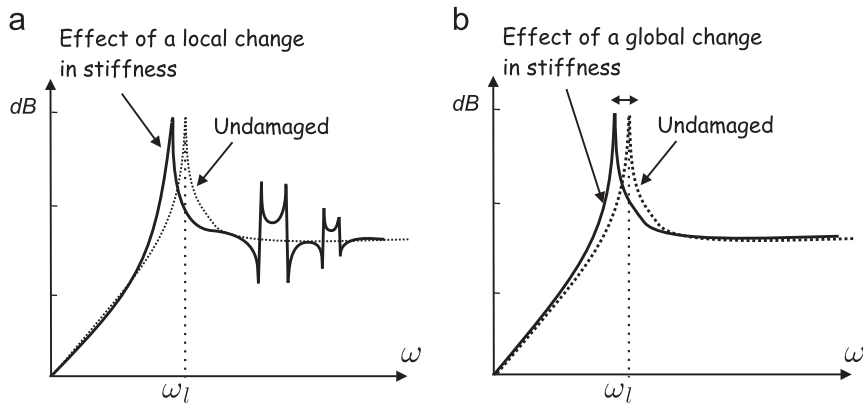
Fig. 2. Effect of a structural change on the modal filter tuned on mode l. (a) Effect of a local stiffness change, (b) effect of a global proportional stiffness change.

pronounced. In particular, for a proportional change of the stiffness or mass matrix, only the eigenfrequencies are affected, without any change in the shape of the mode shapes, so that one gets

$$\sum_{k=1}^{n} \alpha_k c_{ki}^* = \sum_{k=1}^{n} \alpha_k \lambda c_{ki} = \lambda \delta_{li}. \tag{9}$$

As a result, only the eigenfrequency of the modal filter is affected (Fig. 2(b)).

In practice, the linear combiner coefficients α_k should be computed using experimentally identified mode shapes in order to avoid the need to build a numerical model. This can be achieved based on output-only measurements, using for instance stochastic subspace based methods [24–26]. Note that once the α_k coefficients are known, the modal filters are implemented directly in the time domain using Eq. (2), so that the excitation does not need to be measured.

The reduction of data with modal filters has already been studied numerically in [4,6] and experimentally in [38] for damage detection. Section 2.4 details the extension of that idea to damage localization.

2.3. Signal processing for modal filter outputs

If the input force $f(t)$ is known, one can directly compute the FRF of the output of the modal filter $g(t)$ using well established methods for FRF estimation. For random signals, the FRF is typically estimated using the ratio of the power spectra and cross power spectra. Using the H_1 FRF estimator, the estimation of $G(\omega)$ is given by [9]

$$G(\omega) = \frac{S_{gg}(\omega)}{S_{gf}(\omega)}, \tag{10}$$

where $S_{gg}(\omega)$ is the auto-spectral density (or power spectral density—PSD) of the filtered frequency response $g(t)$ and $S_{gf}(\omega)$ is the cross-spectral density of $g(t)$ and the input $f(t)$. These power spectra can be estimated efficiently thanks to Welch's method [19] for instance. If the input force is not known, one can simply compute the power spectral density of $g(t)$. This quantity is directly related to the amplitude of $G(\omega)$ as follows [9]:

$$S_{gg}(\omega) = |G(\omega)|^2 S_{ff}(\omega) \tag{11}$$

This relationship shows that if peaks appear in $|G(\omega)|$, they will also appear in $S_{gg}(\omega)$. On the other hand, if sharp peaks are present in $S_{ff}(\omega)$, they might be interpreted as damage. In practice however, for ambient excitations in civil engineering applications, such peaks are rarely present in the excitation signal. In addition, if the frequencies corresponding to those peaks are not in the frequency bands around the natural frequencies of interest of the system, they can easily be differentiated from peaks appearing due to damage.

In summary, for output-only measurements, it is necessary to detect the appearance of peaks around the natural frequencies of the healthy system in the PSD of $g(t)$. If the input force is known, the same should be applied to the amplitude of the FRF $|G(\omega)|$, as these two quantities are closely related.

2.4. Extension to damage localization

The previous idea can be very easily extended to damage localization. Consider now that the n sensors installed on the structure are grouped in several smaller sensor networks, each consisting of m sensors. Modal filters can be built for each of these local sensor networks resulting in independent *local modal filters*. If the local network I contains sensors $y_{1,I}, \ldots, y_{m,I}$,

the output of its modal filter tuned to mode l is given by

$$g_l(t) = \sum_{k=1}^{m} \alpha_{k,l} y_{k,l}(t), \tag{12}$$

where $\alpha_{k,l}$ coefficients are computed in order to satisfy the following condition:

$$\sum_{k=1}^{m} \alpha_{k,l} c_{(k,l)i} = \delta_{li}, \tag{13}$$

where $c_{(k,l)i}$ is the kth ($k = 1, ..., m$) component of the ith mode shape projected on the lth local sensor network. If a damage occurs under spatial filter l and if the sensor responses are locally sensitive to damage, the mode shape will only be altered in that spatial filter. As a result, only the spatial filter l will have spurious peaks, indicating the location of the damage. The efficiency of the approach relies therefore on a very strong assumption: damage in a local filter will cause a local change of the mode shape which is limited to the very close vicinity of the damage location. Such a property depends on the type of measured quantity which is considered. Earlier studies [20] have shown that in beam-like structures, curvatures exhibit such a property for the first low order mode shapes. A more general discussion has been made in [2], where it was demonstrated that the result can be generalized to any kind of structure using strains instead of curvatures. The importance of using mode shapes with a wavelength much larger than the size of damage was also emphasized. This has been the primary motivation for using strain measurements in several previous works [37,36]. Note however that a similar approach has been proposed in [17] using accelerations. These two approaches will be compared in Section 3.1.

2.5. Practical issues for the computation of the modal filter coefficients

The success of damage localization using modal filters depends directly on the modal filtering quality. If the peak is not sufficiently filtered, it is much more difficult to detect the damage based on the appearance of spurious peaks. Modal filter coefficients are computed from Eq. (5) in which matrix $[C]^T$ is a $N \times n$ matrix. A necessary condition to ensure the compatibility of the N equations is to have at least as many sensors as the number of modes considered for the filtering ($n > N$). If $n = N$, the matrix is square and can be simply inverted. If $n > N$, the matrix is rectangular. In order to compute $\{\alpha_l\}$, a widely applied technique is to use the Moore–Penrose pseudo-inverse of matrix $[C]^T$, usually noted $([C]^T)^\dagger$. The coefficients of the modal filter are then given by

$$\{\alpha_l\} = ([C]^T)^\dagger \{e_l\}. \tag{14}$$

This approach is well suited when the rank of matrix $[C]$ is full (rank $r = N$). There are however situations in which the rank is not full. For modal filters, this is generally the case:

(i) when the sensor network is such that two mode shapes are identical when projected on the sensors (spatial aliasing);
(ii) when the mode shapes have been poorly identified: noise and identification errors can cause a linear dependency of the mode shapes leading to a decrease of the rank;
(iii) when the size of the sensor network decreases (as in the case of local filters): the distinction between the mode shapes becomes more and more difficult, especially for low order mode shapes, which tends to decrease the rank.

When the rank is deficient, it is possible to regularize the inversion of matrix $[C]^T$ using a singular value decomposition (SVD) of the matrix:

$$[C]^T = [U][S][V]^T, \tag{15}$$

where $[U]$ and $[V]$ are unitary matrices and $[S]$ is a rectangular diagonal matrix with the singular values σ_i on the main diagonal ordered in decreasing order. If u_i and v_i are the columns of $[U]$ and $[V]$ respectively, one can rewrite Eq. (15) as follows:

$$[C]^T = \sum_{i=1}^{N} \sigma_i u_i v_i^T, \tag{16}$$

and the pseudo-inverse of $[C]^T$ is given by

$$([C]^T)^\dagger = \left(\sum_{i=1}^{N} \frac{1}{\sigma_i} v_i u_i^T \right) \tag{17}$$

When the rank is deficient, some singular values will be very close to 0 and should be removed from the summation. Otherwise, they will have a predominant contribution due to the $1/\sigma_i$ term. Truncating the sum is necessary to regularize the pseudo-inversion but will result in a reduced number of modes efficiently filtered. In the particular case of local modal filters, rank deficiency is very often present due to the fact that global mode shapes are very similar when projected on small sensor networks, especially for the low order mode shapes. As a result, filtering many mode shapes is often not possible and the application should be restricted to the filtering of only a few (typically two or three) mode shapes.
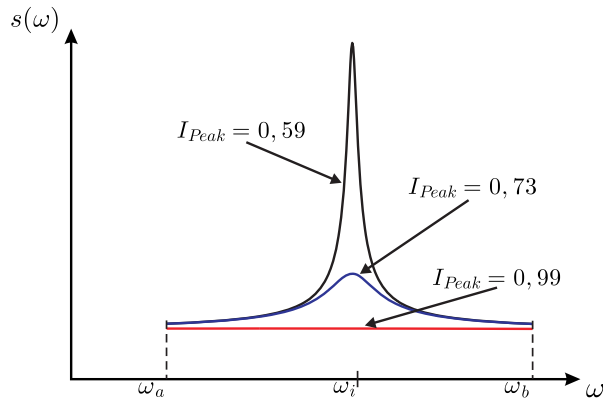
Fig. 3. Example of I_{Peak} values for an increasing peak.

2.6. Feature extraction based on modal filter outputs

Because the spurious peaks are expected to appear around the initial eigenfrequencies of the structure, the strategy consists in extracting one feature in each frequency band around them. Let $s(\omega)$ be the frequency dependent amplitude in the frequency range $[\omega_a, \omega_b]$ (Fig. 3). In this application, $s(\omega)$ is either the amplitude of the FRF of the modal filter $|G(\omega)|$ or the PSD $S_{gg}(\omega)$. The frequency band is typically defined by $\omega_a = 0.95\omega_i$ and $\omega_b = 1.05\omega_i$, where ω_i is the angular eigenfrequency. A peak indicator is then computed in this frequency interval:

$$I_{Peak} = \frac{2\sqrt{3}RVF}{\omega_b - \omega_a}, \tag{18}$$

where RVF is the root variance frequency defined by

$$RVF = \sqrt{\frac{\int_{\omega_a}^{\omega_b} (\omega - FC)^2 s(\omega)\, d\omega}{\int_{\omega_a}^{\omega_b} s(\omega)\, d\omega}}, \tag{19}$$

and FC is the frequency center defined by

$$FC = \frac{\int_{\omega_a}^{\omega_b} \omega s(\omega)\, d\omega}{\int_{\omega_a}^{\omega_b} s(\omega)\, d\omega}. \tag{20}$$

Theoretically, I_{Peak} is equal to 1 if $s(\omega)$ is constant and decreases when the peak grows. Fig. 3 gives an example of I_{Peak} values computed between ω_a and ω_b when a spurious peak grows around ω_i.

In practice however, I_{Peak} might decrease or increase if more than one spurious peak appears in the frequency band of interest (which will occur if two eigenfrequencies are close to each other). The advantage of that feature is that it is sensitive to the peak growth but not to the level of the input. I_{Peak} can therefore be used in an output only approach. More details on the peak indicator computation can be found in [6].

2.7. Automation of the damage localization process

In order to have an efficient damage localization method applicable to any civil engineering structure, there is a need for a very simple but robust way to automatically set off alarms when damage occurs. When the excitations are random, I_{Peak} behaves like a random variable. That feature will therefore follow a statistical distribution which can be inferred from several undamaged samples. Many tools have been developed to detect a change in that statistical distribution such as outlier analysis or hypothesis testing. In this work, we apply the control charts [18,29]. This tool of statistical quality control plots the features or quantities representative of their statistical distribution as a function of the samples. Different univariate or multivariate control charts exist but all these control charts are based on the same principle. In phase I, a set of samples are collected and analyzed to infer statistical characteristics of the process when it is assumed to be in control (i.e. when the structure is undamaged). The aim of this step is to compute the control limits (upper control limit UCL and/or lower control limits LCL) between which the feature should be included if the process stays in control. Those limits are governed by the statistical distribution $f(x)$ of the quality characteristic and the probability $1-\alpha$ that any in control sample will fall inside the control limits. There are control limits that can be computed to detect a shift of the mean value of the process or a shift of the variance of the process.

Once a set of reliable control charts has been established (phase I), the process is under monitoring (phase II). The process state is unknown (it might be in or out of control), and if a sample falls outside the control limits previously computed, it is considered as an abnormal value, and an alarm is triggered. The phase I fixes the probability of type I (false alarms) and type II (missing alarms) errors. Because the control limit values are based on the number of samples in the control set of data, the statistical distribution $f(x)$ and the α value, the statistical analysis must be done very carefully.

In the following examples, several peak indicators will be monitored simultaneously using a single control chart: the multivariate Hotelling T^2 control chart. Consider p features following a p-normal distribution. The Hotelling T^2 control chart monitors the Mahalanobis distance T^2:

$$T^2 = (x-\overline{x})^T \Sigma^{-1} (x-\overline{x}), \tag{21}$$

where Σ is the $p \times p$ estimated covariance matrix of features, x is the current $p \times 1$ feature vector, and $\overline{x}$ is the $p \times 1$ vector of estimated mean values of x vectors (only the undamaged samples are considered to obtain $\overline{x}$). The upper control limit UCL is computed thanks to a F distribution:

$$UCL = \frac{p(m+1)(m-1)}{(m^2-mp)} F_{\alpha, p, m-p}, \tag{22}$$

where p is the number of variables, m is the number of samples in the set of data in phase I, and α is such that there is a probability of $1-\alpha$ that any in control sample will fall between the control limits. If the T^2 distance exceeds UCL, an alarm is set off.

2.8. Summary of the proposed method

Fig. 4 summarizes the application of the automated damage localization using local modal filters:
The successive steps are:

(A) Initialization of the monitoring system: the structure is assumed to be undamaged and this phase needs a very basic user interaction.
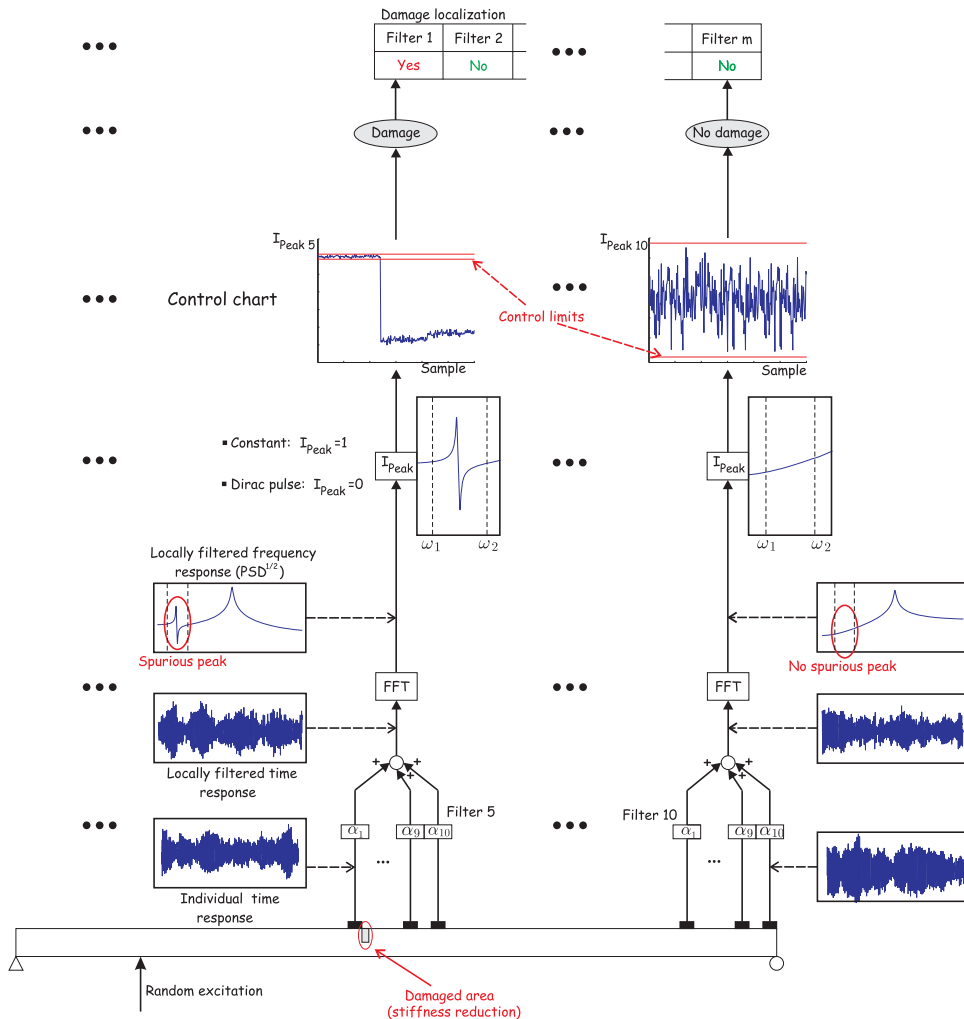(1) Identify the mode shapes as well as the corresponding eigenfrequencies in the bandwidth of interest.

Fig. 4. Flow chart of damage localization using local modal filters.

(2) Choose and compute the modal filter coefficients for each local sensor network (i.e. compute the coefficients $\alpha_{k,l}$ from Eq. (13)).

(3) Extract a set of samples of the feature vector for the undamaged structure:
- measure the responses $g_l(t)$ of each local modal filter (real time linear combination of sensor responses) for a given acquisition time;
- compute the PSD $S_{l,gg}(\omega)$ of each $g_l(t)$;
- extract the peak indicators of interest I_{Peak} from each PSD.

(4) Compute the control limits based on the features (I_{Peak} here) collected for several undamaged samples to apply the control charts: this is the training step.

(B) From here, the system is ready for the monitoring: there is no more user interaction and the structure state is unknown. The data processing is carried out in each local sensor network independently:

(1) Extract the features:
- measure the responses $g_l(t)$;
- compute $S_{l,gg}(\omega)$;
- compute the peak indicators I_{Peak}.

(2) Check if the feature vector composed of the I_{Peak} values of interest falls inside the control limits.

If an alarm is triggered in one of the local sensor networks, damage is detected and assumed to be located in the area covered by the local network. The main advantages of the proposed method are:
- its simplicity and applicability to any kind of structure;
- the possibility to use in-service ambient vibrations;
- the full automation of the process, once the initialization phase has been done;
- the fact that it is a data-based (no model needed) and unsupervised (no need for training data from the damaged structure) method.
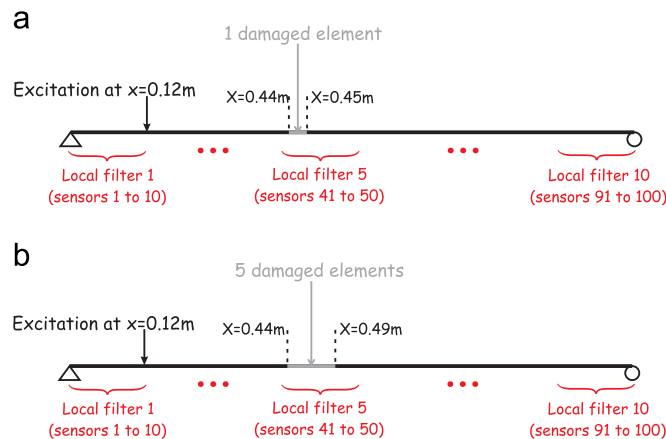
Fig. 5. Location of damages and excitation. (a) Damage introduced in one element, (b) damage introduced in five elements.

Table 1
Damage cases and input signals.

Label	Samples	Level of damage	Input
U	1–120	/	I_1: constant PSD, low amplitude
D_1	121–200	2% in 1 element	I_1
D_2	201–300	4% in 1 element	I_1
U_2	301–420	/	I_2: constant PSD, high amplitude
D_3	421–500	2% in 1 element	I_2
D_4	501–600	4% in 1 element	I_2
U_3	601–700	/	I_3: linearly decreasing PSD, low amplitude
D_5	701–800	2% in 1 element	I_3
D_6	801–900	4% in 1 element	I_3
D_7	901–1000	10% in 1 element	I_1
D_8	1001–1100	20% in 1 element	I_1
D_9	1101–1200	10% in 5 elements	I_1
D_{10}	1201–1300	20% in 5 elements	I_1

3. Application examples

3.1. Comparison of damage localization based on local modal filters using strain measurements and acceleration measurements

This first numerical example deals with the application of the local modal filters on a simply supported beam. The method is tested with strains and accelerations, and the performances obtained for the damage localization are compared.

3.1.1. Description of the case study

The structure investigated is depicted in Fig. 5: It consists of a 1 m × 0.1 m × 0.1 m simply supported concrete beam, modeled with 100 Euler–Bernoulli beam elements under the *Structural Dynamics Toolbox* in *Matlab* [32]. The whole beam is covered with 100 strain/acceleration sensors grouped in 10 local filters of 10 sensors, and it is excited with a point force (band-limited white noise between 0 Hz and 4000 Hz), exciting the first 4 mode shapes of the structure. Damage, in the form of a proportional decrease of the stiffness, is introduced in 1 or in 5 elements as shown in Fig. 5. The different damage scenarios investigated are summarized in Table 1 (the damage is always situated only in local filter 5). In addition, three different types of input signals are considered. The first excitation I_1 has a flat, constant PSD in the frequency band of interest, and a low amplitude level. The second excitation I_2 is similar but its amplitude is multiplied by 100. The last excitation I_3 has a linearly decreasing PSD with an amplitude comparable to I_1.

3.1.2. Computation of the sensor responses

The sensors time responses are obtained thanks to an in-house numerical simulator which is applying a time integration scheme based on Duhamel's formula [22], and which was already used in [5]. A small level of white noise is introduced directly on the sensor responses under the form of Eq. (23), with $\beta = 0.01$:

$$y_k(t) = y_k^0(t) + \beta \lambda \max_{|t}(y_k^0(t)), \tag{23}$$

where $y_k(t)$ and $y_k^0(t)$ are respectively the noisy and non-noisy responses of sensor k ($k = 1, \ldots, 100$) at time t. λ is the random parameter, with its continuous distribution $f(\lambda)$ following a Gaussian distribution with zero mean and unitary standard deviation. Each sample consists of 10 s of measurement, with a sampling rate of 8000 Hz. The coefficients of the local modal filters are computed based on the local mode shapes (using Eq. (17)) identified from the output-only generated time-domain responses using a stochastic subspace identification algorithm implemented in the *Macec* toolbox under *Matlab* [26]). For each local filter, $S_{I,gg}$ is then computed using Welch's method.

3.1.3. Acceleration and strains measurements for damage localization

As discussed earlier, for an optimal damage localization using local modal filters, measurements that are locally sensitive to damage are preferable. Pandey et al. [20] showed that for beams, curvatures exhibit this local sensitivity. In beam structures, the kinematic assumptions are such that the curvatures are proportional to the longitudinal strains at a given height in a section. In general, for any type of structure, this local sensitivity can be generalized for strains, and the localization is improved when the length of the damage is small compared to the wavelength of the mode, as demonstrated numerically in [2] and experimentally by Gu et al. in [13]. In previous works by the authors of this work, it was therefore proposed to use strain sensors in order to detect and localize very small damages [37,36,3]. At the same time, Mendrok et al. have worked on a very similar idea based on local modal filters using acceleration sensors in [17], despite the fact that the effect of damage on accelerations is less clear than with strains. To illustrate that principle, Fig. 6 depicts the impact of damage case D_{10} (decrease of stiffness of 20% in five elements, see Table 1) on the strain and the acceleration first mode shape. The plotted quantity is the relative difference $\Delta\phi_{1i}/\phi_{1i}$ (in %) between the undamaged mode shape and the damaged mode shape at sensor i.

The figure shows that the effect of damage on strains and accelerations is very different. The use of strains sensors is very interesting because the effect of damage is concentrated around the damaged area. With acceleration sensors, the mode shape change is also maximum around the damaged area but the effect is much more spread. From those observations, one could therefore expect that the damage localization will be more accurate with strain sensors. Note also that the $\Delta\phi_{1i}/\phi_{1i}$
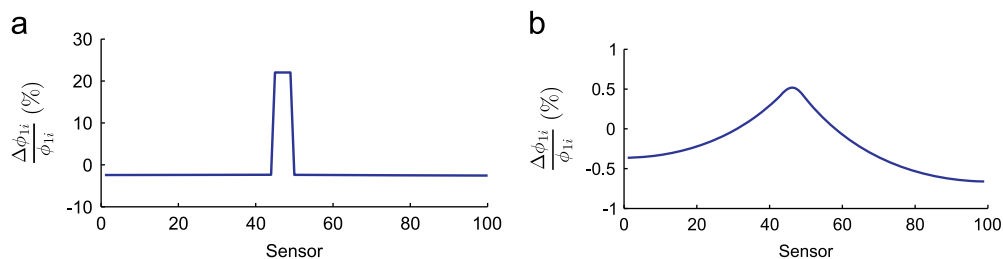

Fig. 6. Impact of damage (case D_{10}) on the mode shapes. (a) First strain mode shape, (b) first acceleration mode shape.

scales differ a lot between the two type of sensors: for the same damage case, the maximum $\Delta\phi_{1i}/\phi_{1i}$ value is 22% for the strains, while it is only 0.5% for the accelerations. It seems therefore that strains are more sensitive to damage, and will lead to an earlier damage localization. A major drawback with the strain sensors is however the fact that, due to the very local nature of the change, if the damaged area is not covered with sensors, it will not be detected and localized.

3.1.4. Effect of damage on the PSDs of local modal filters based on strain or acceleration sensors

Figs. 7–10 show the effect of damage cases D_1 (minimum damage level) and D_{10} (maximum damage level) on $S_{I,gg}(\omega)$ ($I = 5,6$) for a modal filter tuned to mode 2 with strain and acceleration measurements. With strain sensors, peaks appear even for the lowest level of damage in local filter 5 where the damage is present, and no peaks appear in local filter 6. Very strong peaks appear for the highest level of damage. With acceleration sensors, small peaks appear only for the highest level of damage, both in local filters 5 and 6. This clearly shows that if accelerations are used, only high levels of damage can be detected and the localization is not very precise (this point will be better illustrated in Section 3.1.5).

3.1.5. Feature extraction and statistical process control

In this example, the peak indicators used for the feature vector are:

- I_{Peak} computed around f_1 (modal filter tuned on mode 2) and f_2 (modal filter tuned on mode 1) for strain sensors;
- I_{Peak} computed around f_3 (modal filter tuned on mode 1) and f_3 (modal filter tuned on mode 2) for acceleration sensors.

The choice of the peak indicators for strain measurements results directly from the idea of monitoring only the first one or two low order mode shapes for a better localization (as discussed in [2]). As this choice was shown to give very poor results for accelerations, it was decided to take the most favorable peak indicators for a fair comparison, which resulted in the choice described above. In both cases, it results in a bi-dimensional feature vector for each of the local sensor networks. This bi-dimensional feature vector is monitored (independently in each local network) using the Hotelling T^2 multivariate control chart. The control limits are computed using 90/120 of the undamaged samples (case U_1), and the tolerance α is set to 2.5%. Fig. 11 shows this chart for local filters 5 and 6.

As expected, the features based on strain measurements are much more sensitive to damage than the features based on acceleration measurements. For all the damage cases, the feature vector based on strain measurements falls above the control limit, while the feature vector based on acceleration measurements falls above the control limit only for the highest
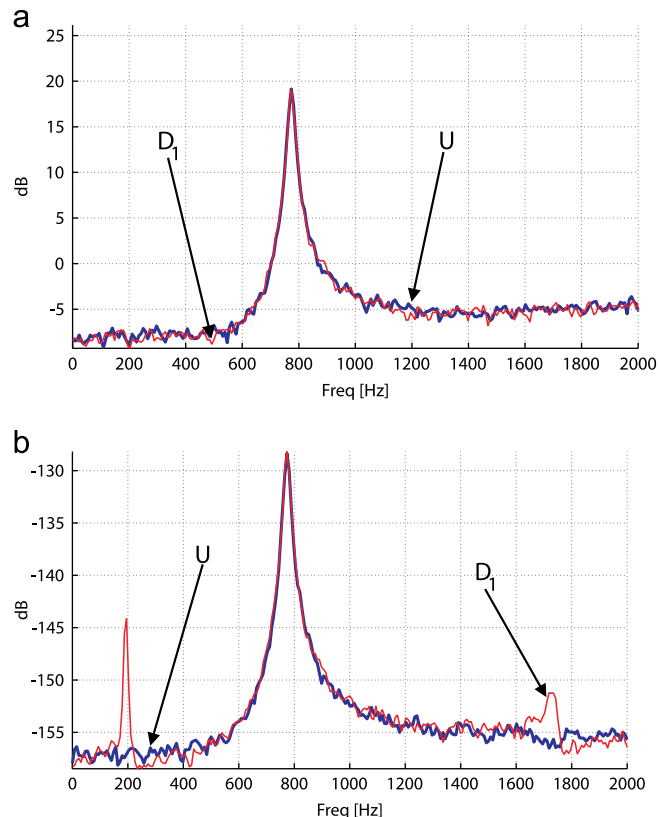

Fig. 7. $S_{5,gg}$ (PSD of modal filter of local sensor network 5) for a tuning on mode 2. Effect of damage case D_1 using (a) acceleration sensors, (b) strain sensors.

Fig. 8. $S_{6,gg}$ (PSD of modal filter of local sensor network 6) for a tuning on mode 2. Effect of damage case D_1 using (a) acceleration sensors, (b) strain sensors.
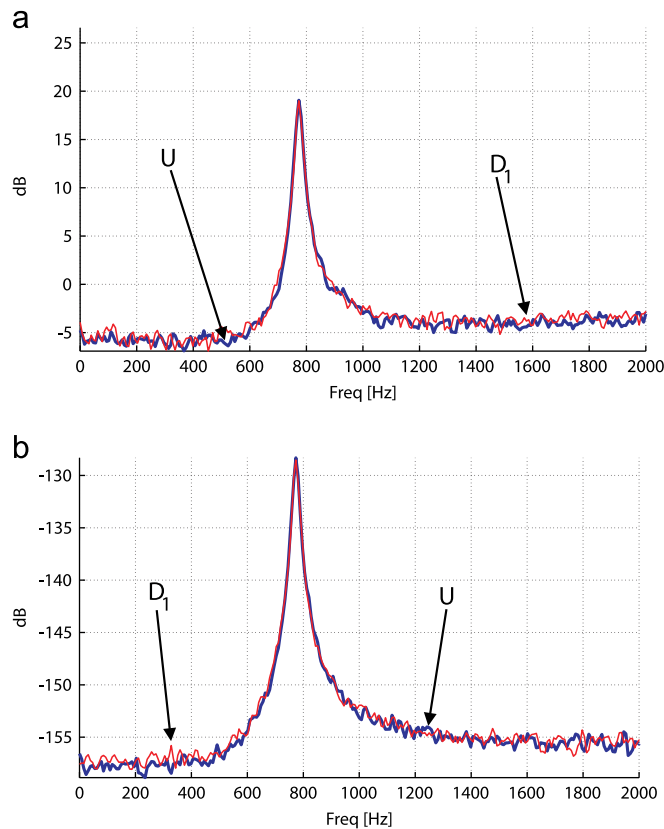
damage cases (cases D_8, D_9 and D_{10}). In addition, because of the small spurious peak around f_3 for local filter 6, there are some false alarms for damage cases D_9 and D_{10} (see Fig. 11(b)).

The summary of all the damage alarms is given in Fig. 12. The figure shows that the damaged area is correctly located using strain sensors, even with different excitation conditions. With acceleration sensors, only the highest damage levels are localized in a much less precise manner (alarms are triggered in local filters 4, 5 and 6, around the true damage localization). This example demonstrates the excellent performances of the method using strain measurements. Very small damages (2% stiffness reduction over an area covering only 1/100th of the total length of the beam) can be correctly detected and localized even with a moderate level of noise added on the measurements.

3.2. Application to a realistic bridge structure using fiber optic long gage dynamic strain sensors

The second case study is a more realistic problem. In this example, the structure investigated is a three-dimensional model of a bridge inspired from the Boirs viaduc near Liège in Belgium. The sensor network is composed of long-gage fiber optic sensors (while in the beam example, the strains were directly computed from the curvatures). Besides noise on sensors, some environmental changes are also introduced in order to assess the robustness of the method.

3.2.1. Description of the case study

Fig. 13 shows the finite element model of the bridge. It is made of concrete and modeled with hexahedral 8-node elements using the *Structural Dynamics Toolbox* [32] under *Matlab*. The bridge is considered as simply supported at its extremities.

The first five natural frequencies computed from the finite element model are given in Table 2.

A unique damage between $z = 17.1$ m and $z = 17.3$ m (Fig. 13) is introduced in the form of a small local stiffness reduction. The reduction of stiffness is a common way to simulate damage and has been used widely by many authors in the SHM community. Of course one might argue that this is a rather simplified macro-scale representation of damage. However, in the present study of concrete cracking, the strain sensors used have a long gage and therefore provide an average measurement of strains which corresponds to this macro-scale. A recent study [42] has shown that in that case, a reduced stiffness model fits very well the results obtained using much more complicated non-linear crack propagation models. This justifies the use of such a simple model in our investigations. The network of dynamic strain sensors is composed of 100 long-gage (0.25 m gage length) dynamic strains sensors installed along a straight line and equally spaced between points
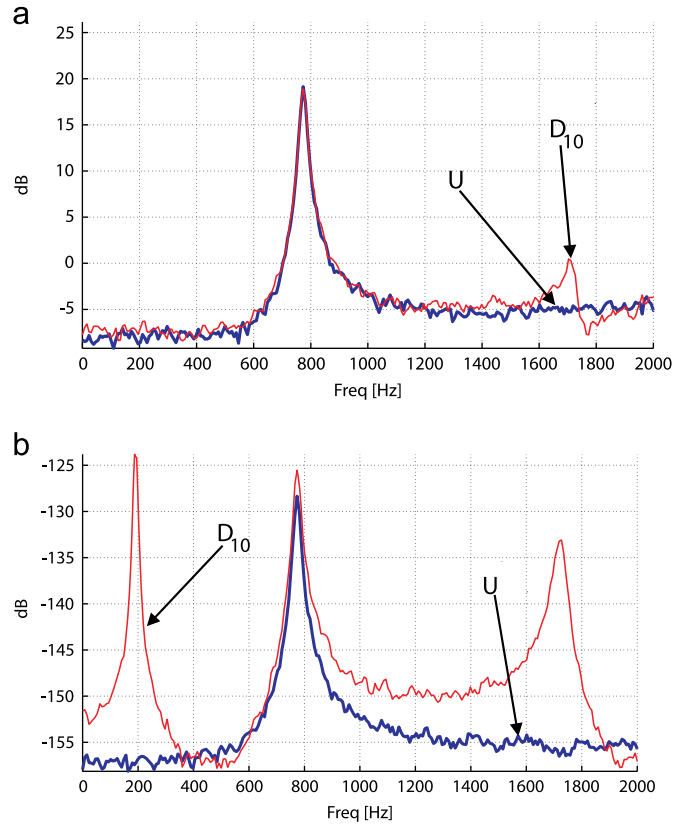
Fig. 9. $S_{5,gg}$ for a tuning on mode 2. Effect of damage case D_{10} using (a) acceleration sensors, (b) strain sensors.
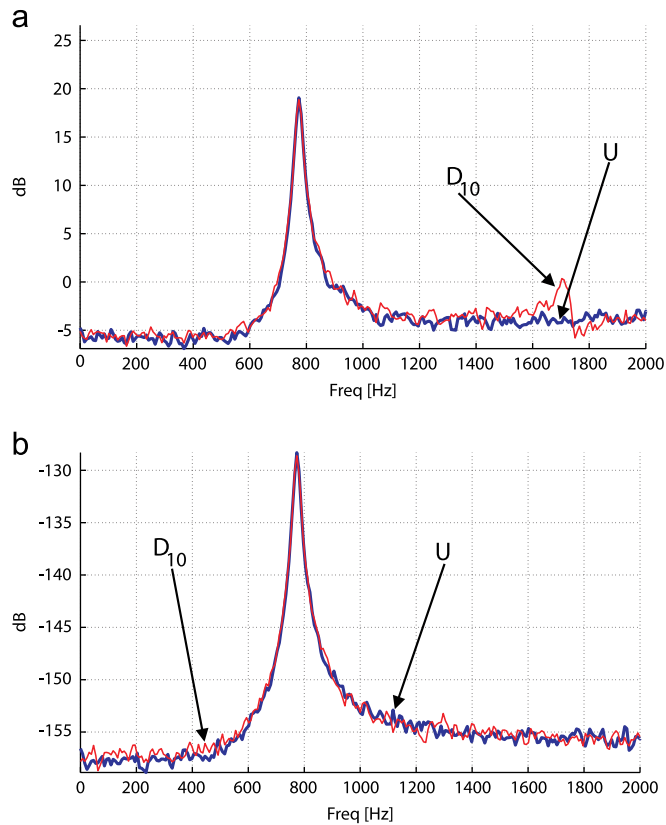

Fig. 10. $S_{6,gg}$ for a tuning on mode 2. Effect of damage case D_{10} using (a) acceleration sensors, (b) strain sensors.
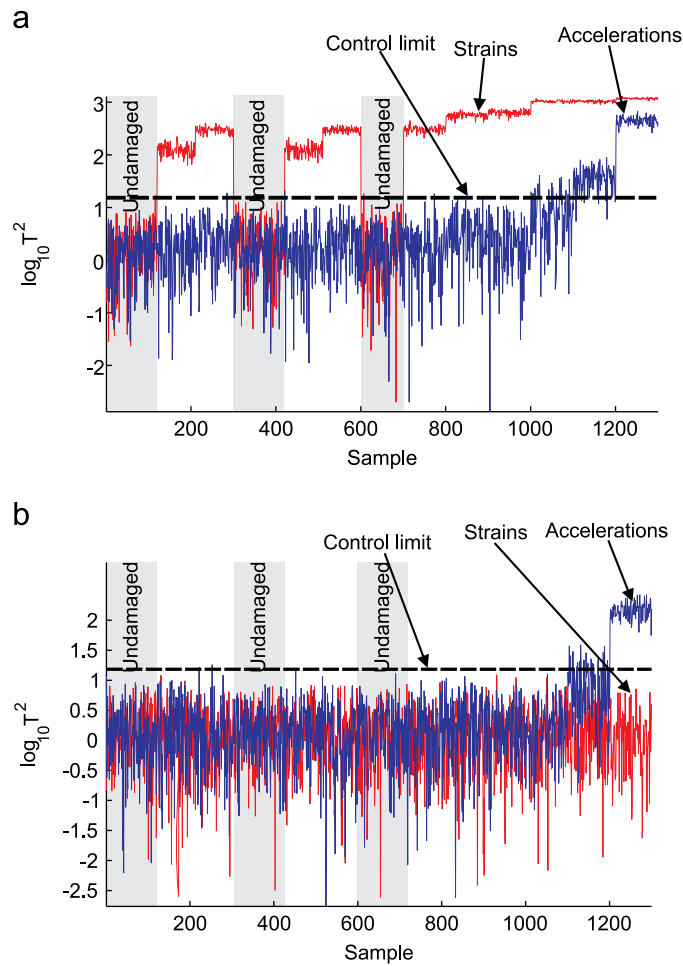
Fig. 11. Hotelling T^2 control chart for strain and acceleration measurements. (a) Local filter 5, (b) local filter 6.

A and B. The bridge is excited with a vertical random force (band-limited white noise) at point C. A small level of white noise is directly added on the sensor responses in the form of Eq. (23), with $\beta = 0.01$. The mode shapes and eigenfrequencies are then identified using the stochastic subspace method implemented in the *Macec* toolbox under *Matlab* based on the sensor responses polluted with noise without any knowledge of the excitation signal. The projection of the first five mode shapes on the strain sensor network is represented in Fig. 14.

The network is then divided into 10 spatial filters, each composed of 10 long-gage fiber optic strain sensors. The damage is located inside local filter 7 (Fig. 15).

The acquisition time for one sample is set to 100 s (with a sampling frequency of 100 Hz). The following damage scenarios are investigated:

(1) no damage (samples 1–100): U;
(2) unique damage with 2% of stiffness reduction (samples 101–200): D_1;
(3) unique damage with 4% of stiffness reduction (samples 201–300): D_2.

Note that the damage is very small: it is less than 1/100th of the total bridge length, with only a few percents of stiffness reduction. The relative changes in the eigenfrequencies computed directly from the finite element model due to the two damage cases D_1 and D_2 are summarized in Table 3. The shifts are so small that they are much lower than the accuracy of modal identification methods, so that damage detection based on eigenfrequencies would be very likely to fail.

For the next samples, some variability in the structure through a linear variation of Young's modulus along the z direction (Fig. 16) is introduced. This global small change of Young's modulus aims at representing a global (non constant) stiffening effect due to a non-uniform temperature variation along the bridge. This variability is responsible for a shift of the eigenfrequencies given in Table 4 which is much higher than the shift due to damage.
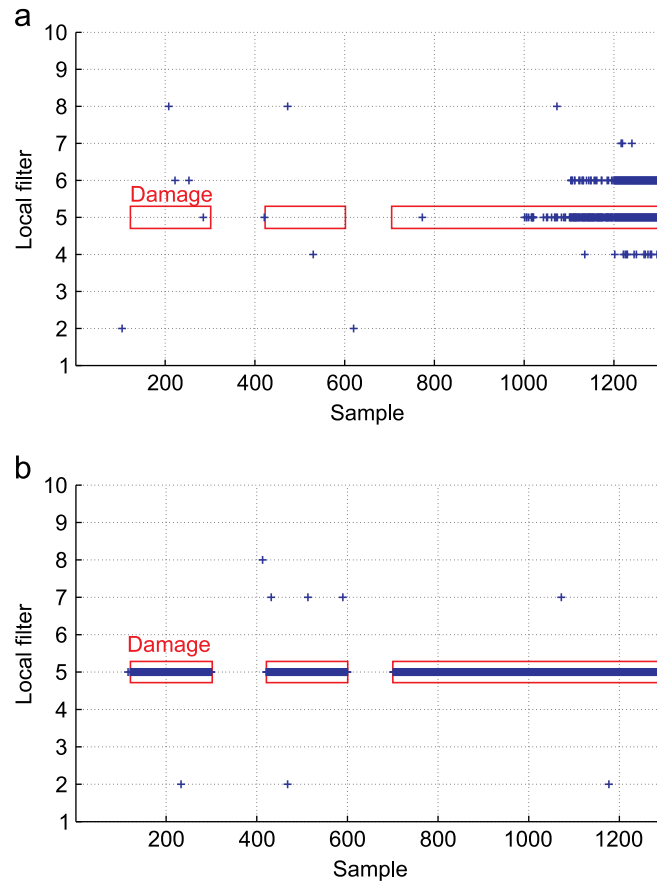
Fig. 12. Summary of damage alerts (true damage cases are surrounded). (a) I_{Peak} with acceleration measurements, (b) I_{Peak} with strain measurements.
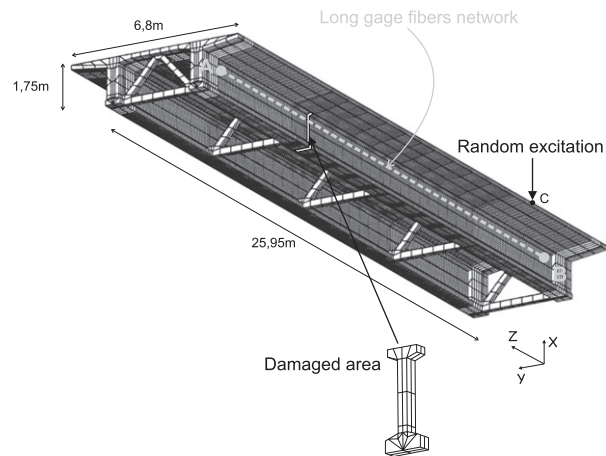
Fig. 13. Finite element model inspired from a real bridge with damaged area and long-gage fiber-optic strain sensors network.

Table 2
Natural frequencies of the undamaged structure (Hz).

f_1	f_2	f_3	f_4	f_5
1.85	4.63	7.22	15.40	16.51
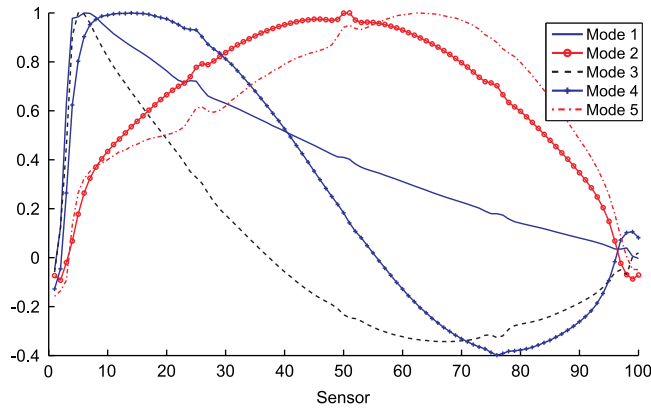
Fig. 14. Projection of the first five mode shapes on the strain sensors network. The modes are identified using output-only measurements polluted with noise.
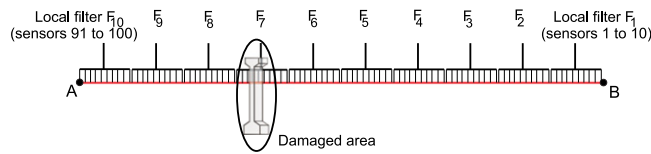
Fig. 15. Spatial filters along the long-gage fiber-optic strain sensors network.

Table 3
Relative change of the eigenfrequencies of the bridge due to damage scenarios D_1 and D_2.

Damage case	Δf_1 (%)	Δf_2 (%)	Δf_3 (%)	Δf_4 (%)	Δf_5 (%)
D_1	−0.0007	−0.0044	−0.0025	−0.0028	−0.0018
D_2	−0.0014	−0.0088	−0.0051	−0.0056	−0.0036
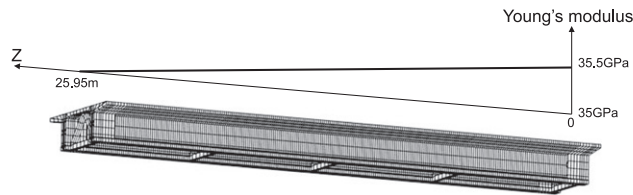
Fig. 16. Value of Young's modulus along the z direction in the bridge representing the variability due to environmental changes.

Table 4
Relative change in the eigenfrequencies of the bridge due to environmental effects (modeled by a linear variation of the stiffness along the bridge).

Δf_1	Δf_2	Δf_3	Δf_4	Δf_5
+0.1501%	+0.3527%	+0.3069%	+0.2857%	+0.2326%

Additional samples are then generated for the following cases:

(1) no damage, with linear stiffness change (samples 301–350): $U_{\Delta T}$;
(2) unique damage with 2% of stiffness reduction, with linear stiffness change (samples 351–400): $D_{\Delta T1}$;
(3) unique damage with 4% of stiffness reduction, with linear stiffness change (samples 401–450): $D_{\Delta T2}$.

3.2.2. Choice of the features for the damage localization

As explained in Section 2.5, the computation of the coefficients of local modal filters can be difficult due to the fact that as the size of the sensor network decreases, the projection of the mode shapes on the local sensor network become more and

more collinear, causing a rank deficiency in matrix $[C]^T$. This is illustrated in Fig. 17 in which the value of $S_{I,gg}(\omega)$ is plotted for a filter tuned on modes 1 and 2 when the size of the local filter decreases. The modal filter coefficients have been computed using 5 mode shapes in matrix $[C]$. The figure clearly shows that the filtering quality strongly decreases when the size of local filters decreases, due to the rank deficiency. If only two mode shapes are considered in matrix $[C]$, the filtering with 10 local filters of 10 sensors is of good quality, but the higher order mode shapes are not filtered (Fig. 18). This is the minimum number of modes to be filtered in order for the method to be applicable, and results in two peak indicators which can be computed.

The effect of damage levels D_1 and D_2 on $S_{7,gg}$ is illustrated for modal filters tuned to modes 1 and 2 in Fig. 19. The figure shows the appearance of small but detectable peaks as the damage grows. In this example, the feature vector is again of dimension 2. The change in the feature vector can be represented in a two-dimensional space, as shown in Fig. 20. The figure
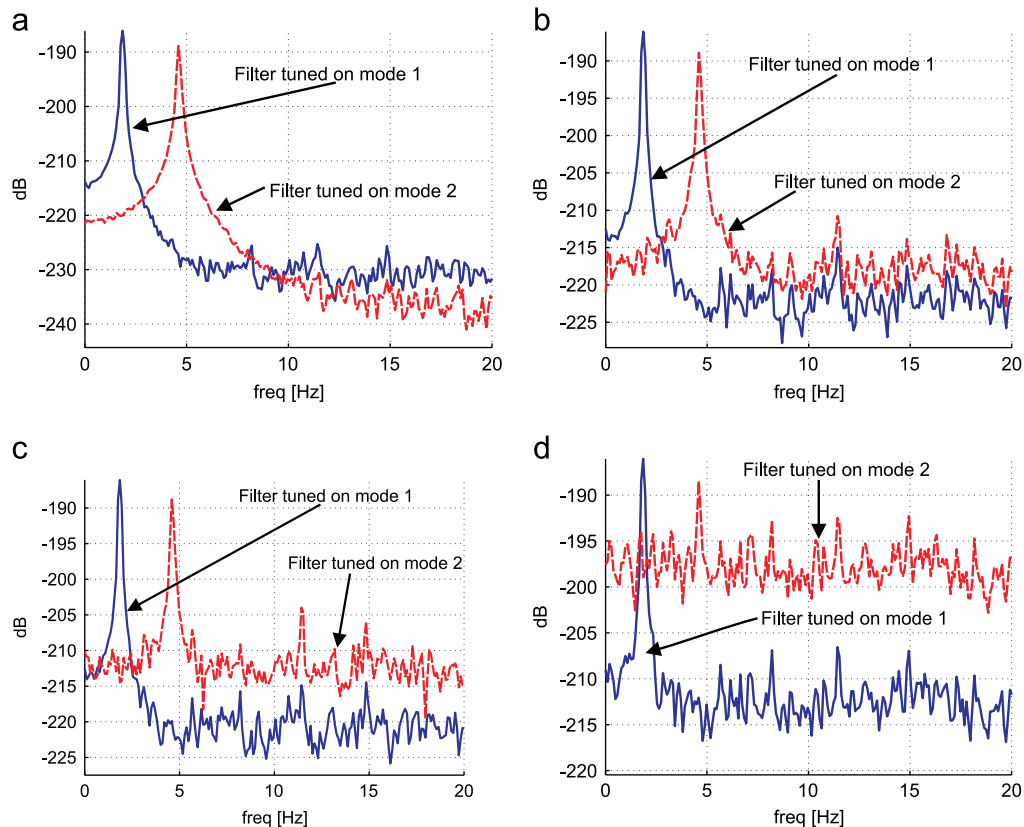
Fig. 17. Effect of the size of the local filters on the filtered frequency responses (filter F_1). Matrix $[C]$ contains 5 mode shapes. (a) 1 global filter of 100 sensors, (b) 2 local filters of 50 sensors, (c) 5 local filters of 20 sensors, (d) 10 local filters of 10 sensors.
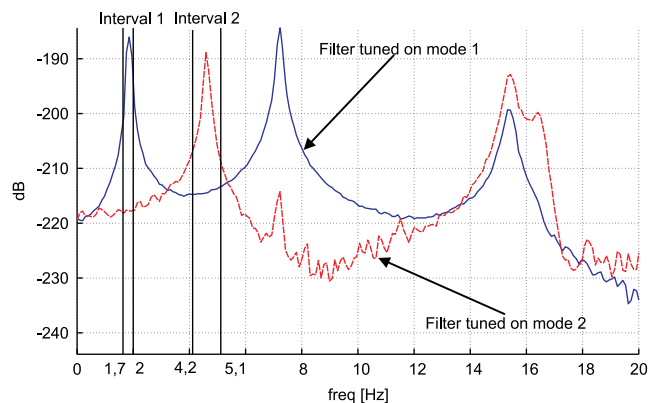
Fig. 18. Modal filtering taking into account only the first two mode shapes in matrix $[C]$ (filter F_1 for 10 local filters of 10 sensors).
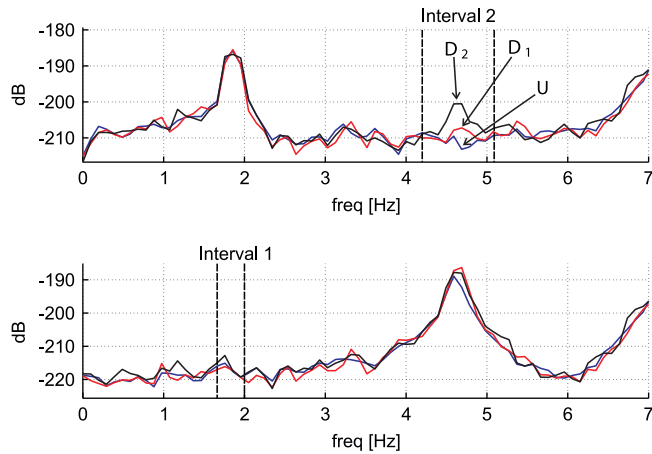
Fig. 19. Growth of spurious peaks in interval 2 (top) and 1 (bottom).
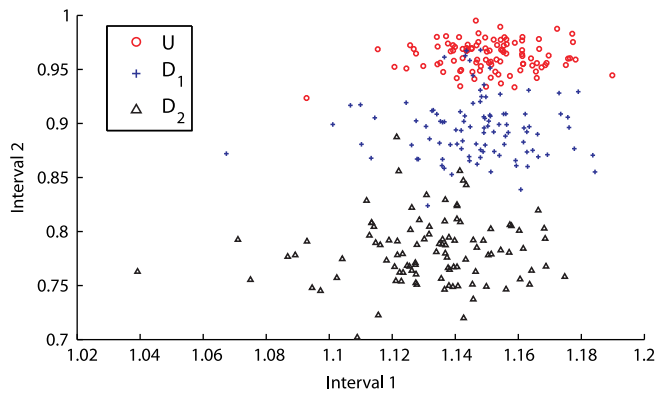
Fig. 20. 2D plot of features for local filter F_7 (first 300 samples).
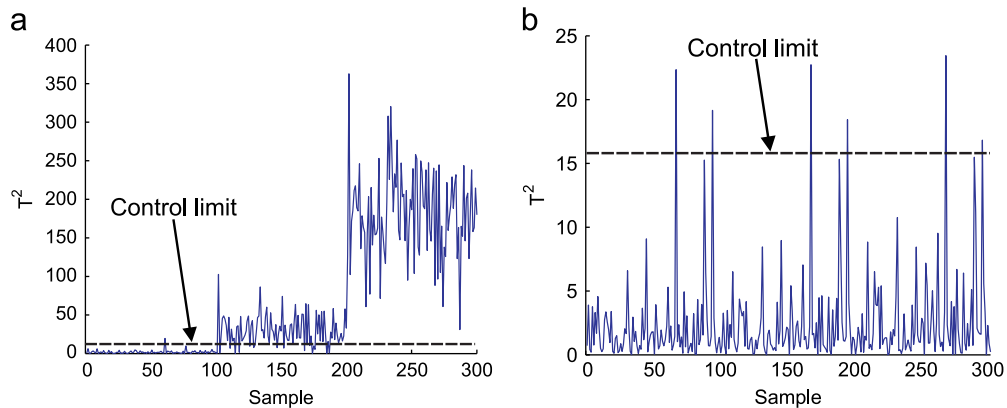
Fig. 21. Application of the Hotelling T^2 control charts on filters F_7 and F_8. (a) Hotelling T^2 control chart for filter F_7, (b) Hotelling T^2 control chart for filter F_8.

shows a clear shift of the cloud of points from the undamaged to the two damaged cases, with a higher sensitivity of the second feature (second peak on the first modal filter).

An approximatively normal distribution has been observed for the two peak indicators in all the local modal filters so that the use of the Hotelling T^2 control chart is adequate.

3.2.3. Automated damage localization

Fig. 21 illustrates the application of Hotelling T^2 control chart for filter F_7 (which includes the damaged area) and filter F_8, just next to the damaged area for the first 300 samples (no environmental changes). The tolerance α is once again set to 2.5%, as in Section 3.1.5.

Fig. 22. Summary of the damage alerts for all the filters (true damage cases are surrounded).

The damage alarms are summarized in Fig. 22, showing that the damage localization succeeded for both levels of damage D_1 and D_2.

For cases U and $U_{\Delta T}$, only 3 and 4 isolated false alarms are respectively triggered. These can easily be differentiated from damage which causes continuous alarms in the control chart. A damage of 2% of stiffness reduction is less clearly located with a linear change of stiffness (there are 20/50 correct alarms in damage case $D_{\Delta T1}$ and 77/100 correct alarms in damage case D_1), but the results are still satisfying. The damage of 4% of stiffness is correctly located (no alarm is missing), even with environmental changes, in both cases D_2 and $D_{\Delta T2}$. The results confirm the excellent performances of the method on a more realistic type of structure. Very small damages are correctly detected and located even in the presence of variability in the baseline structure. Such small levels of damage could not be detected using eigenfrequencies, as their changes are much smaller than the accuracy of modal identification methods. An adequate choice of the features (dynamic strains) coupled to a local processing approach is believed to be the key point for the success and performance of the proposed method.

4. Conclusion

In this paper, a novel method for automated data-based damage localization is proposed. The method requires an initialization phase in which the mode shapes of the structure are identified based on ambient vibration records from a large network of sensors. The mode shapes are then used to construct very simple and fast signal processing algorithms for real-time feature extraction. The main steps of the signal processing are (i) a linear combination of the sensors signals (whose coefficients depend on the identified mode shapes), (ii) the computation of the power spectral density of the resulting signal, (iii) the computation of peak indicators in given frequency bands. This methodology has been previously proposed for damage detection and the subject of the present work is its extension to damage localization. In order to do so, the large network of sensors is divided into smaller independent units, and the feature extraction procedure is applied independently in each local network. The change of the feature vector is monitored using control charts. The main idea of the method is that by using dynamic strain measurements which are locally sensitive to damage, damage will have an effect on the features extracted in the local filter in which damage has appeared only, giving the indication of the location of the damage. After the initialization phase, the monitoring phase is fully automated and does not require any user interaction.

The performances of the proposed method have been illustrated on two numerical examples: a simply supported beam, and a three-dimensional bridge structure. In both examples, the excellent performances of the method have been demonstrated. Levels of damage as low as 2% stiffness reduction in an area covering only 1/100th of the size of the structure have been successfully detected and localized, even in the presence of moderate levels of noise and variability in the baseline condition. The authors believe that the performances of the method can be explained by (i) the choice of the sensing technology (dynamic strain sensors) and (ii) the local nature of the processing of the data.

Future work will be focused on (i) the assessment of the performances of the method based on numerical simulations including more realistic damage models [3], (ii) the determination of the optimal size of the local sensor networks with respect to the size and level of the damage to be detected and (iii) experimental application and validation of the method.

Acknowledgments

References

[1] T.G. Chondros, A.D. Dimarogonas, Influence of cracks on the dynamic characteristics of structures, J. Vib. Acoust. Stress Reliab. Design 111 (1989) 251–256.

[2] A. Deraemaeker, On the use of dynamic strains and curvatures for vibration based damage localization, in: Proceedings of the Fifth European Workshop on Structural Health Monitoring, Sorrento, Italy, 2010, pp. 835–840.

[3] A. Deraemaeker, Assessment of damage localization based on spatial filters using numerical crack propagation models, in: Proceedings of the Ninth International Conference on Damage Assessment of Structures, Oxford, United Kingdom, 2011.

[4] A. Deraemaeker, A. Preumont, Vibration based damage detection using large array sensors and spatial filters, Mech. Syst. Signal Process. 20 (2006) 1615–1630.

[5] A. Deraemaeker, E. Reynders, G.D. Roeck, J. Kullaa, Vibration-based structural health monitoring using output-only measurements under changing environment, Mech. Syst. Signal Process. 22 (2008) 34–56.

[6] A. Deraemaeker, K. Worden, New Trends in Vibration Based Structural Health Monitoring, Springer Wien, New York, 2010.

[7] S.W. Doebling, C.R. Farrar, M.B. Prime, A summary review of vibration-based damage identification methods, Shock Vib. Dig. 30 (1998) 91–105.

[8] E.E. Dubin, B.S. Yanev, Managing the East River bridges in New York City, in: Proceedings of 7th International Symposium on Smart Structures and Materials, Newport Beach, CA, USA, 2001, pp. 60–74.

[9] D.J. Ewins, Modal Testing: Theory and Practice, Research Studies Press LTD, Letchworth, 1984.

[10] C.R. Farrar, S.W. Doebling, D.A. Nix, Vibration-based structural damage identification, Philos. Trans.: Math. Phys. Eng. Sci. Math. 259 (2001) 131–149.

[11] C.R. Farrar, S.W. Doebling, P.J. Cornwell, E.G. Straser, Variability of modal parameters measured on the Alamosa canyon bridge, in: Proceedings of 15th International Modal Analysis Conference, Orlando, FL, USA, 1997, pp. 257–263.

[12] C.P. Fritzen, D. Jennewein, T. Kiefer, Damage detection based on model updating methods, Mech. Syst. Signal Process. 12 (1998) 163–186.

[13] Y. Gu, L. Tong, P. Tan, Surface strain distribution method for delamination detection using piezoelectric actuators and sensors, in: Proceedings of 9th International Conference on Damage Assessment of Structures, Oxford, UK, 2011.

[14] C. Hellier, Handbook of Nondestructive Evaluation, McGraw-Hill, New York, 2003.

[15] J. Kullaa, Distinguishing between sensor fault, structural damage, and environmental or operational effects in structural health monitoring, Mech. Syst. Signal Process. 25 (2011) 2976–2989.

[16] J.P. Lynch, K.J. Loh, A summary review of wireless sensors and sensor networks for structural health monitoring, Shock Vib. Dig. 38 (2006) 91–128.

[17] K. Mendrok, T. Uhl, Experimental verification of the damage localization procedure based on modal filtering, Struct. Health Monit. 10 (2) (2011) 157–171.

[18] D.C. Montgomery, Statistical Quality Control: A Modern Introduction, John Wiley and Sons, New York, 2009.

[19] A.V. Oppenheim, R.W. Schafer, Digital Signal Processing, Prentice-Hall, New Jersey, 1975.

[20] A.K. Pandey, M. Biswas, M.M. Samman, Damage detection from changes in curvature mode shapes, J. Sound Vib. 145 (1991) 321–332.

[21] D. Pines, E. Aktan, Status of Structural Health Monitoring of long-span bridges in the United States, Progr. Struct. Eng. Mater. 4 (2002) 372–380.

[22] A. Preumont, Frequency domain analysis of time integration operators, Earthquake Eng. Struct. Dyn. 10 (1982) 691–697.

[23] E. Reynders, G.D. Roeck, Damage identification on the Tilff bridge by vibration monitoring using finite element model updating, in: Proceedings of Experimental Vibration Analysis for Civil Engineering Structures, Bordeaux, France, 2005, pp. 49–59.

[24] E. Reynders, G.D. Roeck, Reference-based combined deterministic-stochastic subspace identification for experimental and operational modal analysis, Mech. Syst. Signal Process. 22 (2008) 617–737.

[25] E. Reynders, R. Pintelon, G.D. Roeck, Uncertainty bounds on modal parameters obtained from stochastic subspace identification, Mech. Syst. Signal Process. 22 (2007) 948–969.

[26] E. Reynders, M. Schevenels, G.D. Roeck, MACEC 3.1: A Matlab Toolbox for Experimental and Operational Modal Analysis, Report BWM-2010-05, Department of Civil Engineering, K.U.Leuven, 2010.

[27] E. Reynders, A. Teughels, G.D. Roeck, Finite element model updating and structural damage identification using OMAX data, Mech. Syst. Signal Process. 24 (2010) 1306–1323.

[28] K. Rofidal, U.S. coast guard responds following the collapse of the I-35W bridge in Minnesota, USCG Reservist 54 (2007) 26–29.

[29] T.P. Ryan, Statistical Methods for Quality Improvement, John Wiley and Sons, New York, 2000.

[30] A. Rytter, Vibration Based Inspection of Civil Engineering Structures, University of Aalborg, 1993.

[31] O.D. Salawu, Detection of structural damage through changes in frequency: a review, Eng. Struct. 19 (1997) 718–723.

[32] SDTools, Structural Dynamic Toolbox ⟨http://www.sdtools.com⟩.

[33] SensorsMag, Sensors Magazine ⟨http://www.sensorsmag.com⟩.

[34] H. Sohn, C.R. Farrar, F. Hemez, D. Shunk, D. tinemates, B. Nadler, A Review of Structural Health Monitoring Literature from 1996–2001, Los Alamos National Laboratory Report LA-13976-MS, 2004.

[35] G. J Stein, Some recent developments in acceleration sensors, Meas. Sci. Rev. 1 (2001) 183–186.

[36] G. Tondreau, A. Deraemaeker, Damage localization in bridges using multi-scale filters and large strain sensor networks, in: Proceedings of ISMA2010, Leuven, Belgium, 2010, pp. 1477–1490.

[37] G. Tondreau, A. Deraemaeker, Vibration based damage localization using multi-scale filters and large strain sensor networks, in: Proceedings of the Fifth European Workshop on Structural Health Monitoring, Sorrento, Italy, 2010, pp. 895–900.

[38] G. Tondreau, A. Deraemaeker, E. Papatheou, Experimental damage detection using modal filters on an aircraft wing, in: Proceedings of Eurodyn2011, Leuven, Belgium, 2011, pp. 2083–2089.

[39] Q. Zhang, R.J. Allemang, D.L. Brown, Modal filter: concept and application, in: Proceedings of 8th International Modal Analysis Conference, Hyatt Orlando FL, USA, 1990, pp. 487–496.

[40] S.J. Shelley, J.F. Schultze, R.W. Rost, R.J. Allemang, Active vibration control utilizing a discrete modal filter based control technique, in: Proceedings of ISMA1992, Leuven, Belgium, 1992.

[41] G.L. Slater, S.J. Shelley, Health monitoring of flexible structures using modal filter concepts, in: Proceedings of SPIE Smart Structures and Materials, Albuquerque, NM, USA, 1993, pp. 997–1008.

[42] M. Brehm, T.J. Massart, A. Deraemaeker, Modeling of concrete cracking for the design of SHM systems: comparison of implicit gradient damage models and simplified linear representations, in: Proceedings of Framcos 2013, Toledo, Spain, March 2013.